5358 *Chem. Mater.* **2009,** *21,* 5358–5364
DOI:10.1021/cm901227e

CHEMISTRY OF MATERIALS
Article

Stabilization of Metal Nanoparticles in Cubic Mesostructured Silica and Its Application in Regenerable Deep Desulfurization of Warm Syngas

Liyu Li,* David L. King, Jun Liu, Qisheng Huo,† Kake Zhu, Chongmin Wang, Mark Gerber, Don Stevens, and Yong Wang

Institute for Interfacial Catalysis, Pacific Northwest National Laboratory, Post Office Box 999, Richland, Washington 99354. †*Current address: College of Chemistry, Jilin University, Changchun, 130023 (China).*

Received May 4, 2009. Revised Manuscript Received September 11, 2009

Metal and metal oxide nanoparticles supported on high surface area materials are widely used in industry for fuel and chemical production and for environmental pollution control, but preventing nanosized particle sintering has remained a great challenge. In this paper, we report that Ni−Cu alloy nanoparticles can be effectively stabilized in cubic mesostructured silica (SBA-16) following a conventional impregnation and thermal treatment process. The three-dimensional interconnected cage structure of the mesoporous SBA-16 allows good accessibility of reactant gas molecules to the metal nanoparticles and confines these particles within its nanosized cages. This confinement hinders metal nanoparticle migration and sintering under harsh conditions. A new class of regenerable metal-based adsorbents which can remove sulfur impurities from warm syngas stream down to less than 60 parts per billion by volume (ppbv) is described. This same confinement strategy is expected to have impact for minimizing sintering or particle coarsening of nanosized materials employed in other applications.

Introduction

Mesoporous silicas have been widely investigated as metal catalyst supports because of their high surface area, chemical inertness, and well-controlled pore architectures.[1] In most cases, hexagonal straight pore structures (MCM-41, SBA-15, etc.) have been studied. For these systems, migration and sintering of metal catalyst particles is a common problem due to the straight channel pore structure.[2−4] Moreover, the mesopores can be blocked by the metal particles if they grow to dimensions similar to the pore diameter. Recently, cubic structured three-dimensional mesoporous silicas (SBA-16, SBA-1, HOM-9, KIT-6) have been used as supports for metal, metal oxide, and metal sulfide catalysts.[5−9] Improved catalyst activities were achieved because these structures are more resistant to pore blocking and allow fast transport of reactants and products. In this work, we report that the cubic mesoporous support can effectively stabilize metal nanoparticles within its cage structure, and a class of regenerable metal-based sulfur adsorbents has been developed using SBA-16 as support.

SBA-16 comprises close-packed spherical empty cages (see Figure 1).[10,11] The cages have a body-centered cubic symmetry (*Im*3*m*). Each cage is connected to eight neighboring cages by narrow openings. The dimension of the cages and the openings can be adjusted by the synthesis conditions.[12] This material should be superior to two-dimensional hexagonally structured mesoporous silicas for stabilizing nanoparticles, by "locking" them inside the interconnected cages. Also, compared to other mesoporous silica materials, SBA-16 has better thermal stability, which is a prerequisite for applications involving high temperature operation or treatment.[13]

The effectiveness of this unique structure for preventing nanoparticles from sintering was examined through design of a regenerable metal-based adsorbent for warm syngas deep sulfur removal. Gasification of coal or biomass to syngas followed by catalytic synthesis of liquid hydrocarbons or oxygenates provides a feasible strategy to meet the increasing demand for transportation fuels.

*To whom correspondence should be addressed. E-mail: liyu.li@pnl.gov.

(1) Taguchi, A.; Schüth, F. *Microporous Mesoporous Mater.* **2005**, *77*, 1–45.
(2) Sietsma, J. R. A.; Meeldijk, J. D.; Versluijs-Helder, M.; Broersma, A.; van Dillen, A. J.; de Jongh, P. E.; de Jong, K. P. *Chem. Mater.* **2008**, *20*, 2921–2931.
(3) Sietsma, J. R. A.; Friedrich, H.; Broersma, A.; Versluijs-Helder, M.; van Dillen, A. J.; de Jongh, P. E.; de Jong, K. P. *J. Catal.* **2008**, *260*, 227–235.
(4) Yang, C. M.; Kalwei, M.; Schüth, F.; Chao, K. J. *Appl. Catal., A* **2003**, *254*, 289–296.
(5) Vinu, A.; Krithiga, T.; Murugesan, V.; Hartmann, M. *Adv. Mater.* **2004**, *16*(20), 1817–1821.
(6) Park, Y.; Kang, T.; Lee, J.; Kim, P.; Kim, H.; Yi, J. *Catal. Today* **2004**, *97*, 195–203.
(7) Soni, K.; Rana, B. S.; Sinha, A. K.; Bhaumik, A.; Nacdi, M.; Kumar, M.; Dhar, G. M. *Appl. Catal., B* **2009**, *90*, 55–63.
(8) El-Safty, S. A.; Kiyozumi, Y.; Hanaoka, T.; Mizukami, F. *Appl. Catal., A* **2008**, *337*, 121–129.
(9) El-Safty, S. A.; Kiyozumi, Y.; Hanaoka, T.; Mizukami, F. *Appl. Catal., B* **2008**, *82*, 169–179.
(10) Zhao, D. Y.; Huo, Q. S.; Feng, J. L.; Chmelka, B. F.; Stucky, G. D. *J. Am. Chem. Soc.* **1998**, *120*, 6024–6036.
(11) Sakamoto, Y.; Kaneda, M.; Terasaki, O.; Zhao, D. Y.; Kim, J. M.; Stucky, G. D.; Shin, H. J.; Ryoo, R. *Nature* **2000**, *408*, 449–453.
(12) Kim, T. W.; Ryoo, R.; Kruk, M.; Gierszal, K. P.; Jaroniec, M.; Kamiya, S.; Terasaki, O. *J. Phys. Chem. B* **2004**, *108*, 11480–11489.
(13) Kruk, M.; Hui, C. M. *J. Am. Chem. Soc.* **2008**, *130*, 1528–1529.

Published on Web 10/22/2009

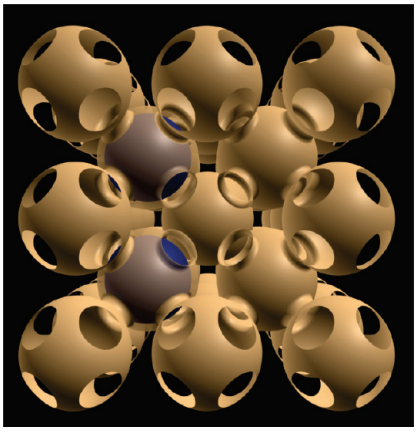

Figure 1. Schematic illustration of the interconnected cage structures of SBA-16, with some small particles trapped inside the cages. The cubic cell size is chosen to contain three cages on each side, and the cell is viewed from a [100] orientation. The space outside the cages is filled with SiO_2 (not shown).

A significant challenge is posed by sulfur present in the syngas, which poisons the catalysts even at low parts per million by volume (ppmv) levels.[14,15] Although technical approaches exist for removal of sulfur species to the required level of <60 ppbv,[16] they are rather costly and energy intensive, employing solvents at ambient or lower temperature[17] and backup sacrificial adsorbents.[18] Since catalytic processes for the production of fuels and chemicals typically operate in the range of 200−300 °C, a process capable of removing sulfur at such an intermediate temperature range is preferred. Several warm and hot sulfur cleanup technologies have been developed in the past years,[19,20] primarily based on zinc oxide-containing materials.[21−25] Fresh ZnO absorbents can remove both H_2S and COS from wet warm syngas down to less than 100 ppb level at temperatures <300 °C, which is controlled by the thermodynamics of the reaction $ZnO + H_2S = ZnS + H_2O$.[25,26] However, the recent pilot-scale warm syngas desulfurization work using a ZnO-based absorbent shows that sulfur can only be removed over regenerated zinc oxide absorbents to a few ppmv, insufficient for chemical synthesis work.[27,28] Deep sulfur removal from warm syngas can be achieved by using the excellent gettering ability of metals (Ni, Cu, Fe) toward sulfur gases, the same reason for their readily being poisoned when used as synthesis catalysts.[29−31] The use of metal-based sulfur getters has been exploited thus far only for sacrificial adsorbents.[32] Development of regenerable metal adsorbents has been stymied by the strong tendency of the metals to sinter or aggregate during the regeneration process, which causes loss in metal surface area and sulfur adsorption capacity. The isolation and stabilization of the small metal particles in cubic structured mesoporous silica SBA-16, as proposed in this work, is intended to allow regeneration of the sulfur-loaded adsorbents with minimal sintering and loss of capacity.

Experimental Section

Adsorbent Preparation. SBA-16 was prepared according to published procedures using poly(ethylene oxide)−poly(propylene oxide)−poly(ethylene oxide) triblock copolymers as supramolecular templates.[10−12] In a typical preparation of SBA-16, triblock copolymer mixtures [0.5 g of P123 ($EO_{20}PO_{70}EO_{20}$) and 2.3 g of F127 ($EO_{106}PO_{70}EO_{106}$)] were dissolved in 130 mL of 2 M HCl at room temperature. To this mixture, 10 g of tetraethylorthosilicate (TEOS) was added, and the mixture was stirred at 40 °C for 20 h. The subsequent hydrothermal treatment was carried out at 100 °C under static conditions for 24 h. The solid product was filtered and dried at 50 °C without washing. For removing the template, the solid was calcined in air at 500 °C for 4 h.

SBA-15 was also prepared according to published procedures.[33] In a typical preparation, 12.0 g of P123 was dissolved in 360 mL of 2 M HCl aqueous solution at 40 °C. Then 25.5 g of TEOS was added to the resulting milky solution, which was then stirred for 18 h at the same temperature. The mixture was transferred into a Teflon-lined autoclave and heated at 100 °C for 24 h without stirring. The white precipitate was filtered, dried in air, and finally calcined at 550 °C for 6 h.

Nickel and nickel−copper mixtures were loaded into SBA-16 and SBA-15 supports by mixing 10 mL of metal nitrate aqueous solution with 1.0 g of support followed by rotary evaporation at 80 °C to dryness and calcination in air at 250 °C for 4 h. The amounts of nickel (16 wt %) and Ni−Cu (a combined 28.8 wt % at Ni to Cu molar ratio of 9 to 1) loaded into the SBA-16 were selected for proof-of-principle and were not optimized for ultimate application. At these loading levels, channel blocking could be minimized and sulfur-containing molecules could freely transport through the interconnected pore structure. Also, use of a modest metal loading increased the probability that the majority of the Ni−Cu particles would be located inside the cage structure. Figure 2 provides a schematic illustration of the process used in this work for stabilizing metal nanoparticles

(14) Bartholomew, C. H. *Appl. Catal., A* **2001**, *212*, 17–60.
(15) Kritzinger, J. A. *Catal. Today* **2002**, *71*, 307–318.
(16) Stiegel, G. J.; Clayton, S.; Der, V. Gasification technologies project portfolio: gas cleaning & conditioning. http://www.netl.doe.gov/technologies/coalpower/gasification (2007).
(17) Hochgesand, G. *Ind. Eng. Chem.* **1970**, *62*(7), 37–43.
(18) Rostrup-Nielsen, J. R.; Sehested, J.; Norskov, J. K. *Adv. Catal.* **2002**, *46*, 65–139.
(19) Gangwal, S. K.; Gupta, R.; McMichael, W. J. *Heat Recov. Syst. CHP* **1995**, *15*(2), 205–214.
(20) Torres, W.; Pansare, S. S.; Goodwin, J. G.Jr. *Catal. Rev.* **2007**, *49*, 407–456.
(21) Jothimurugesan, K.; Gangwal, S. K. *Ind. Eng. Chem. Res.* **1998**, *37*, 1929–1933.
(22) Siriwardane, R. V. U.S. Patent 5,866,503, **1999**.
(23) Gupta, R. P.; Turk, B. S.; Portzer, J. W.; Cicero, D. C. *Environ. Prog.* **2001**, *20*, 187–195.
(24) Slimane, R. B.; Williams, B. E. *Ind. Eng. Chem. Res.* **2002**, *41*, 5676–5685.
(25) Novochinskii, I. I.; Song, C. S.; Ma, X. L.; Liu, X. S.; Shore, L.; Lampert, J.; Farrauto, R. J. *Energy Fuels* **2004**, *18*, 576–583.
(26) Li, L.; King, D. L. *Catal. Today* **2006**, *116*(4), 537–541.
(27) Turk, B.; Schlather, J. Field Testing of a Warm-Gas Desulfurization Process in a Pilot-scale Transport Reactor System. Presented at Gasification Technologies Conference, Oct. 2006, Washington, D.C.
(28) Turk, B.; Albritton, J.; Trembly, J.; Gupta, R.; Toy, L.; Presler-Jur, P.; Schlather, J.; Gibson, J.; Keller, J. Development of a Warm Syngas Clean-up Technology Platform for Power and Chemicals Production. Presented at Pittsburgh Coal Conference, Oct. 2008, Pittsburgh, PA.
(29) Rostrup-Nielsen, J. R.; Pedersen, K. *J. Catal.* **1979**, *59*, 395–404.
(30) McCarty, J. G.; Wise, H. *J. Chem. Phys.* **1980**, *72*(12), 6332–6337.
(31) McCarty, J. G.; Wise, H. *J. Chem. Phys.* **1982**, *76*(2), 1162–1167.
(32) Rostrup-Nielsen, J. R.; Sehested, J.; Norskov, J. K. *Adv. Catal.* **2002**, *47*, 65–139.
(33) Zhao, D. Y.; Feng, J. L.; Huo, Q. S.; Melosh, N.; Fredrickson, G. H.; Chmelka, B. F.; Stucky, G. D. *Science* **1998**, *279*, 548–552.

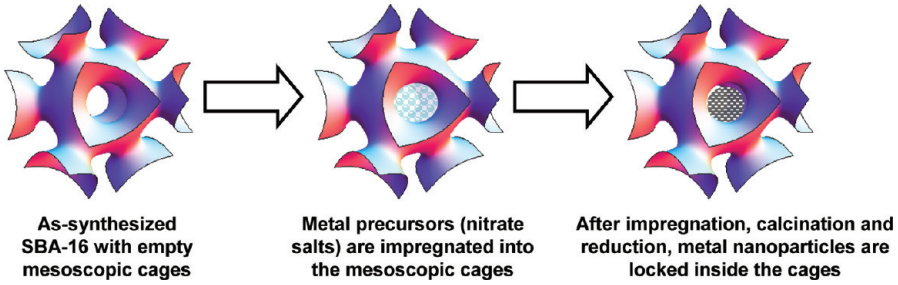

Figure 2. Schematic illustration of the impregnation and thermal treatment process for stabilizing metal nanoparticles in the cage structure of SBA-16.

in SBA-16. As shown in Figure 2, the size of metal nanoparticles is limited by the diameter of the cages in SBA-16.

Ni on fumed SiO_2 and Ni on γ-Al_2O_3 adsorbents, used for comparison, were prepared by incipient wetness of commercial SiO_2 and Al_2O_3 with a $Ni(NO_3)_2$ aqueous solution followed by calcination in air at 500 °C for 4 h. All as-prepared adsorbents were pressed and sieved to obtain 80−100 mesh particles prior to the desulfurization tests.

Desulfurization Test. In a typical desulfurization test, about 0.20 g of 80−100 mesh adsorbent was loaded into a 4.0 mm i.d. Sulfinert coated stainless steel tube and reduced at 500 °C in 50 mL/min 5% clean dry syngas flow for 5 h. The temperature was lowered to 300 °C and then simulated coal or biomass syngas was introduced into the reactor at 12 000 h^{-1} gas hourly space velocity (GHSV) flow rate. The sulfur level in the off-gas was continuously monitored using an Agilent 6890N gas chromatograph coupled with a model 355 sulfur chemiluminescent detector (SCD, Sievers Instruments), which has a sulfur sensitivity of about 20 ppbv. In some tests, the syngas composition change during sulfur removal was monitored by an Agilent Quad Series micro gas chromatograph. Typical regeneration was carried out in a reverse flow mode at 550 °C using a five-cycle alternative "oxidation−reduction" treatment of pure H_2 and 10% air in Ar at 24 000 h^{-1} GHSV with a 3 min purge with Ar between oxidation and reduction treatment. All the desulfurization and regeneration tests were run at atmospheric pressure.

Adsorbent Characterization. Powder X-ray diffraction (XRD) measurement and analysis were conducted with a Philips PW3050 diffractometer using Cu Kα radiation and JADE, a commercial software package. Sample powders were mounted in a front-loading, shallow-cavity zero-background quartz holder, and the data were collected from 5° to 90° 2θ in step-scan mode using steps of 0.02°. The nitrogen BET surface area and adsorption and desorption isotherms were measured with a QUANTACHROME AUTOSORB 6-B gas sorption system at 77 K with degassed samples. Scanning electron microscopy (SEM) analysis was carried out with a JEOL JSM-5900LV microscope. Transmission electron microscopy (TEM) analysis was carried out with a JEOL JEM 2010F microscope. Selected area energy dispersive X-ray spectroscopy (EDS) was performed on regions of interest using a Links EDS system equipped on the microscope. To obtain TEM images, the adsorbent powder was embedded in a resin and cut using a microtone. The cut samples were then dispersed in acetone solution and deposited on a Cu−carbon grid.

Results and Discussion

Figure 3a shows the SEM image of SBA-16, and Figures 3b−f show SEM and TEM images of a 28.8 wt % Ni−Cu/SBA-16 adsorbent before reduction. Ni alone is an effective sulfur adsorbent, but adding Cu to form the alloy improves Ni reducibility and also minimizes Ni methanation and carbon formation activity.[34] SEM analysis of undoped SBA-16 shows typical spherical morphologies for the SBA-16 materials. Some faceted surfaces can be also observed (Figure 3a). Figure 3b shows that not all the metal oxide particles are loaded inside the cages; some are deposited on the surface (white dots in Figure 3b). TEM analysis shows that the nano-sized metal oxide particles (~15 nm) are rather uniformly distributed inside the cages. After in situ reduction, these metal oxide particles are reduced to metal particles. Because the densities of Ni and Cu metals are higher than those of their metal oxides, Ni−Cu metal nanoparticles of ~10 nm size will be produced during the in situ reduction. As a result, these metal particles only partially fill the large cages of the SBA-16 support. It can be seen from Figure 3, at 28.8 wt % Ni−Cu loading level, that less than 25% of the large pores in SBA-16 are occupied.

A simulated biomass-derived syngas containing 36 ppm H_2S (representative of low sulfur biomass syngas), 50% H_2O, 18% H_2, 12% CO, 10% CO_2, 6% CH_4, and 4% He (with the latter being the carrier gas for H_2S) was used for the desulfurization tests, which were carried out at 300 °C with a syngas flow rate of 12 000 h^{-1} GHSV. Figure 4 shows the performance of this adsorbent through five desulfurization and regeneration cycles. The duration of a typical desulfurization step was ~40 h, and that for a typical regeneration step was ~20 h. A steady performance with < 60 ppbv sulfur slip in the treated gas and ~3 wt % sulfur capacity was observed throughout this five cycle test. This indicates that sintering and agglomeration of the metal nanoparticles during the harsh desulfurization and regeneration cycles were effectively inhibited. Assuming all the surface metal atoms are available for S chemisorption and the metal-to-S ratio is 2, only about 0.6 wt % sulfur can be adsorbed for full surface coverage. Therefore the formation of bulk metal sulfides must also occur. According to thermodynamics, under the above test condition, nickel can remove sulfur down to 0.7 ppmv via the reaction $3Ni + 2H_2S = Ni_3S_2 + 2H_2$, and copper can remove sulfur down to 3 ppmv via the reaction $2Cu + H_2S = Cu_2S + H_2$. XRD analysis confirms the presence of a small amount of bulk Ni sulfide (Figure 5). To explain both the high capacity and the low sulfur levels in the exit gas during the desulfurization procedure, a combination of bulk metal

(34) Tavares, M. T.; Alstrup, I.; Bernardo, C. A.; Rostrup-Nielsen, J. R. *J. Catal.* **1996**, *158*, 402–410.

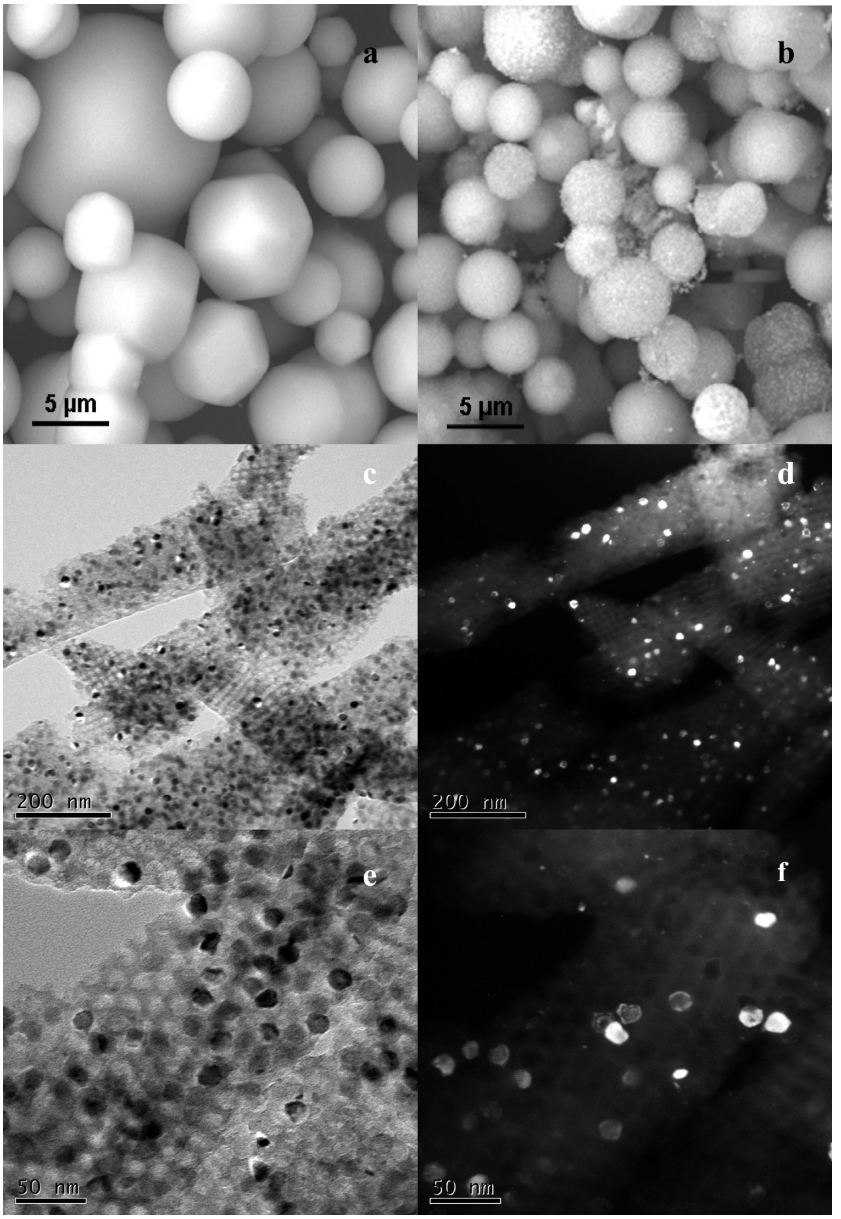

Figure 3. Electron microscope images of a fresh Ni−Cu/SBA-16 adsorbent (metals are in oxide form): a, SEM image of undoped SBA-16; b, SEM image of fresh 28.8 wt % Ni−Cu/SBA-16. Some metal oxide particles (white dots) are deposited on the surface of SBA-16 particles. Pictures c−f: TEM images of 28.8 wt % Ni−Cu/SBA-16 adsorbent. Images c and e are bright-field and d and f are dark-field (same area as of c and e, respectively).

sulfide formation at the front end of the bed and metal surface chemisorption in the latter portion of the bed must be involved. We observe that the measured overall capacity (~3 wt %) is much lower than the theoretical capacity through bulk sulfide formation (~10 wt %), indicating that the kinetics of metal sulfide formation are insufficiently rapid to allow full utilization of the metal. No syngas composition change was observed via gas chromatograph analysis during the desulfurization process.

Figure 6 provides SEM and TEM images of the regenerated adsorbent (in oxide form) after five cycles of operation (~300 h in total). SEM analysis shows that the small metal oxide particles initially covering the outer surface of SBA-16 have agglomerated and sintered, which is consistent with previous understanding of sacrificial sulfur adsorbents: the small metal or metal oxide particles cannot be stabilized by simply using high surface area supports. However, TEM analysis shows the particles inside SBA-16 cages have remarkable stability against sintering. As compared with the fresh samples, no change in the particle sizes, morphologies, and distribution were observed. This excellent stability is attributed to the unique structure of SBA-16, in which the particles are trapped in the cages and cannot diffuse through the small pore openings connecting the cages.

Figure 7 gives N_2 adsorption isotherms of SBA-16, fresh Ni−Cu loaded SBA-16, and regenerated Ni−Cu/SBA-16. Loading the 28.8 wt % Ni−Cu into the pore structure of SBA-16 significantly decreased its BET surface area (from 806 to 166 m^2/g) and pore volume (from 0.82 to 0.27 cm^3/g). However, consistent with the TEM results, minimal changes were observed in the isotherms for the Ni−Cu loaded SBA-16 sample after five cycles of desulfurization and regeneration.

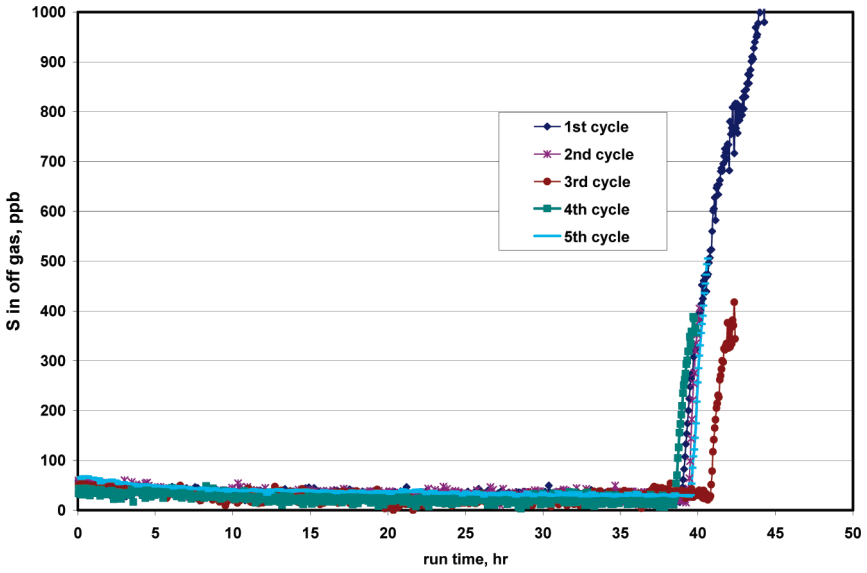

Figure 4. Performance of 28.8 wt % Cu−Ni/SBA-16 as a regenerable sulfur adsorbent for deep sulfur removal from warm biomass syngas.

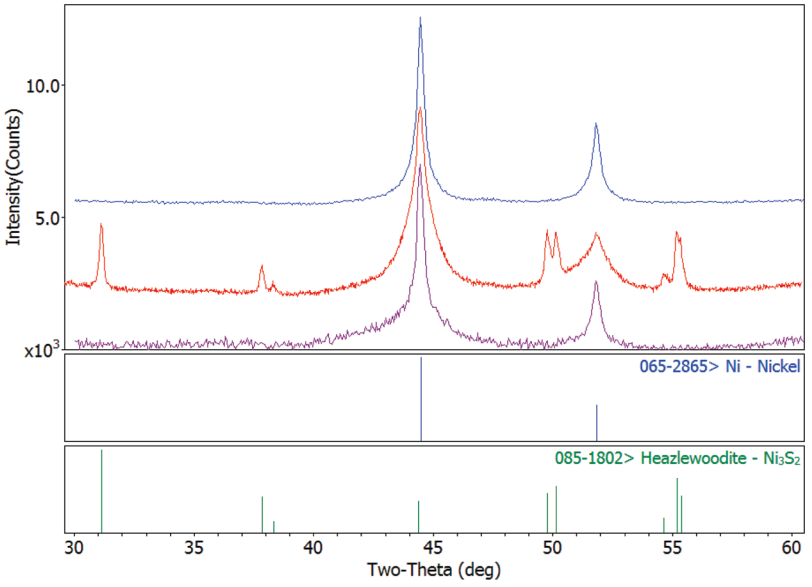

Figure 5. XRD patterns of fresh (top), sulfur-loaded (middle), and regenerated (bottom) 28.8 wt % Cu−Ni/SBA-16 adsorbent.

The SBA-16 support also effectively stabilized pure Ni nanoparticles within its cage structure. For comparison, we synthesized several different 16.6 wt % Ni-containing adsorbents using other high surface area supports, including hexagonally structured mesoporous silica SBA-15, commercial fumed SiO_2, and γ-Al_2O_3. The results are summarized in Table 1. A blank test was run using SBA-16 without any nickel. No sulfur removal was observed. Ni supported on fumed SiO_2 showed some regenerable sulfur capacity. However, this capacity is low because large Ni particles are present, and it is easy for the Ni particles to agglomerate and grow during regeneration. Ni supported on γ-Al_2O_3 gave a nonregenerable 1.5 wt % capacity under tested conditions. Nickel supported within a different mesoporous SiO_2 (two-dimensional hexagonal SBA-15) gave very high first cycle sulfur removal capacity (3 wt %), but the adsorbent could not be regenerated. TEM analysis (Figure 8) confirmed that nickel loaded into the hexagonal channels as very fine particles. However, after adsorption and regeneration, the nickel particles were found to have migrated out of the mesopore structure and sintered. This observation is consistent with previous work.[1−4]

Conventional ZnO-based absorbents typically have more than 20 wt % regenerable sulfur capacity in syngas H_2S and COS cleanup applications. Since the sulfur removal capacities of the trapped metal nanoparticle adsorbents reported here are relatively low, the utility of these materials deserves some comment. A major shortcoming of regenerated ZnO-based adsorbents is that the residual sulfur gas levels exiting the absorbent bed are unacceptably high (several ppmv).[27,28] An integrated system with a ZnO-based absorbent in a bed upstream and the Ni−Cu/SBA-16 adsorbent in a bed downstream as a polisher would give both high sulfur capacity and low sulfur slip in a fully regenerable sulfur sorption system.

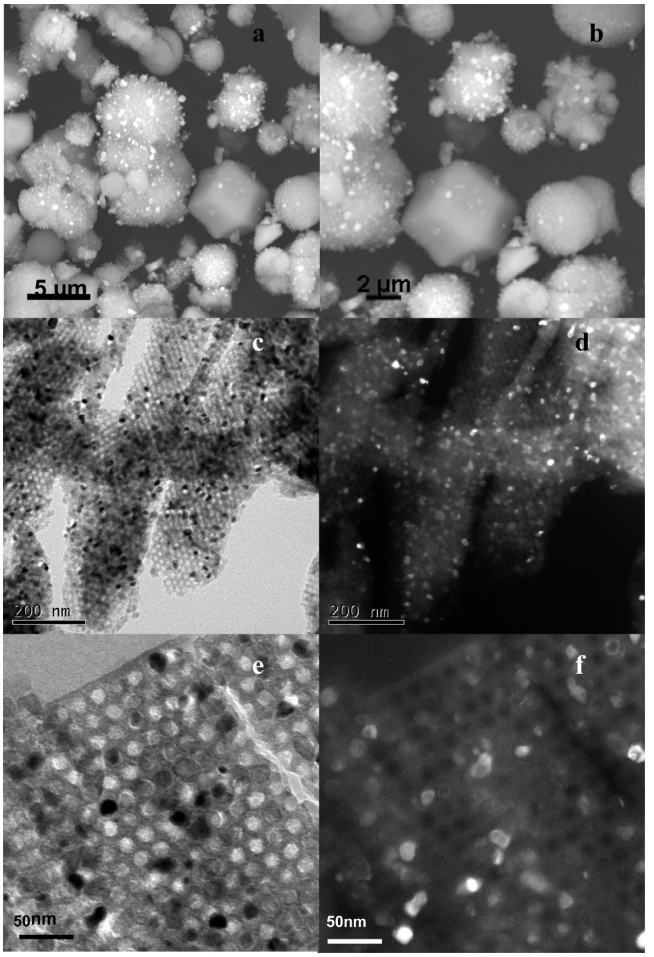

Figure 6. Structure of used 28.8 wt % Ni−Cu/SBA-16 adsorbent (metals are in oxide form). a, b SEM images. c−f, TEM images. Images c and e are bright-field images; d and f are dark-field images.

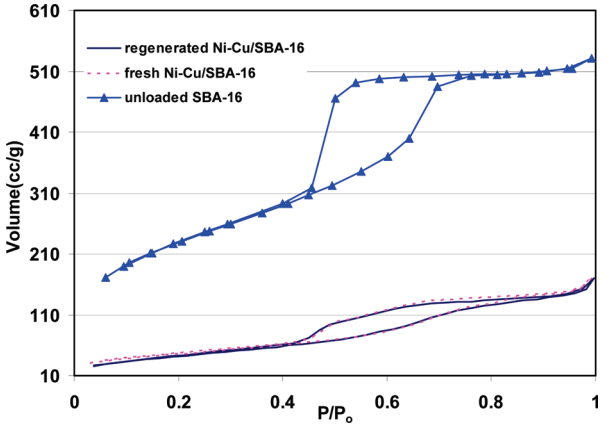

Figure 7. Nitrogen adsorption isotherms of SBA-16, fresh 28.8 wt % Ni−Cu/SBA-16, and regenerated Ni−Cu/SBA-16.

Assuming the sulfur level in the syngas exiting the ZnO bed is 5 ppm, at a typical space velocity of 5000 h^{-1} (liters gas per liter adsorbent per hour), the 3 wt % sulfur capacity of this absorbent (density ~ 0.86 g/cm^3) will allow it to last 680 h before a regeneration is required.

Although mesoporous SBA-16 is not a commercial product, the synthesis is similar to that employed in zeolite production. If such materials were produced in a large scale, their cost can be anticipated to be similar to that of zeolites. As a result, the major part of the absorbent cost could come from the Ni and Cu trapped

Table 1. Sulfur Removal Performance of Ni-Based Adsorbents[a,b]

adsorbent	capacity before 100 ppb sulfur breakthrough, (g S)/(g adsorbent) × 100, %	Regenerability
SBA-16	<0.01%	N/A
16.6 wt % Ni on fumed SiO_2	0.45% for 1st cycle	partially regenerable
	~0.22% for 2nd to 4th cycle	
16.6 wt % Ni on SBA-15	~3% for 1st cycle	not regenerable
	~0% for 2nd cycle	
16.6 wt % Ni on γ-Al_2O_3	~1.5% for 1st cycle	not regenerable
	~0% for 2nd cycle	
16.6 wt % Ni on SBA-16	~0.7% for 5 cycles	regenerable

[a] Surface area of supports: SBA-16, 760 m^2/g; SBA-15, 850 m^2/g; fumed SiO_2, 200 m^2/g; γ-Al_2O_3, 220 m^2/g. [b] Sulfur removal conditions: T = 300 °C; coal syngas composition: 23% H_2, 29% CO, 8% CO_2, 30% H_2O, 10% He, 10 ppm H_2S; flow rate: 12,000 h^{-1} GHSV.

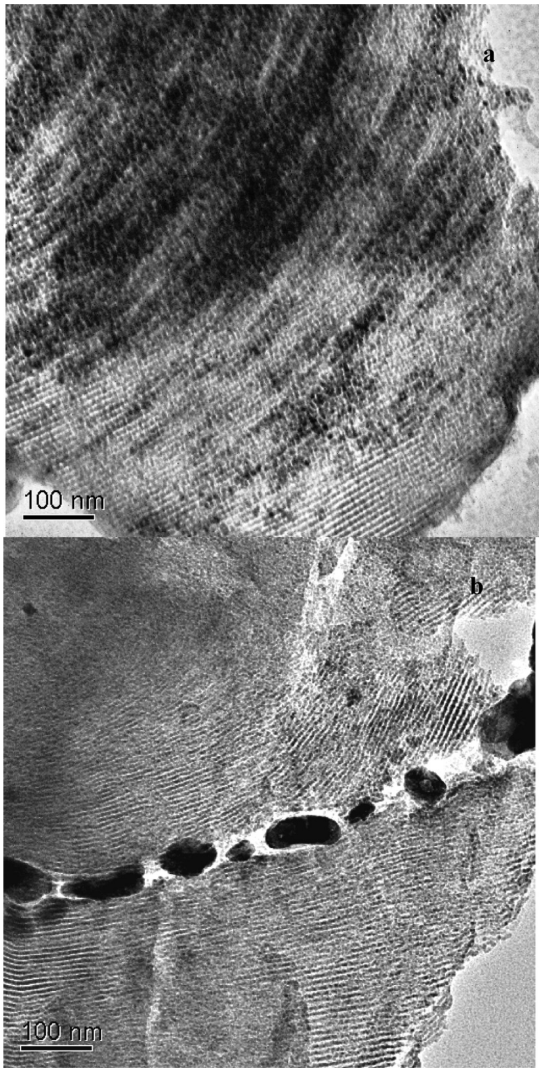

Figure 8. TEM images of (a) fresh and (b) regenerated 16.6 wt % Ni/SBA-15 adsorbent.

in the cages. The amounts of nickel and copper loaded into the SBA-16 support were selected for proof-of-principle, and substantial flexibility remains regarding total metal loading and composition. Optimization of metal loading and other system parameters are topics for future study. The same concept may also find application for removal of other trace level contaminants in processes involving metal catalysts that are susceptible to poisoning.

Conclusions

Three-dimensional mesoporous silica SBA-16 can effectively stabilize metal nanoparticles inside its cage structure. By loading and trapping Ni−Cu nanoparticles in SBA-16 using a conventional impregnation and thermal treatment process, we have demonstrated a class of regenerable metal-based adsorbents that can remove sulfur from warm biomass syngas to less than 60 ppbv with ~3 wt % capacity. This solid adsorbent-based warm deep desulfurization approach can provide economic advantages compared with existing solvent-based technologies and may find use for warm cleanup of gasifier-derived syngas for synthesis applications and of hydrocarbon fuel reformates for fuel cell applications. This work provides new insights into the stability of nanoparticles within controlled mesostructures, opening up many potential applications.

Acknowledgment. This work was performed in part at the Interfacial and Nano Science Facility in the William R. Wiley Environmental Molecular Sciences Laboratory, a national scientific user facility sponsored by the Office of Biological and Environmental Research of the U.S. Department of Energy and located at the Pacific Northwest National Laboratory (PNNL). PNNL is operated for the U.S. Department of Energy by Battelle. The authors wish to acknowledge financial support from the Laboratory Directed Research and Development Program at the PNNL and the Biomass Energy Technology Program of the U.S. Department of Energy. L.L. thanks Dr. F. Gao (PNNL) for preparing Figure 2.